Supporting Information

Anchoring V_2O_5 Nanosheets on Hierarchical Titanium Nitride Nanowire Arrays to Form Core-Shell Heterostructures as Superior Cathode for High-Performance Wearable Aqueous Rechargeable Zinc-Ion Batteries

Qiulong Li[+], Qichong Zhang[+], Chenglong Liu, Zhengyu Zhou, Chaowei Li, Bing He, Ping Man, Xiaona Wang, Yagang Yao*

Materials

Titanium tetrachloride (TiCl$_4$, 99%), zinc sulfate heptahydrate (ZnSO$_4$·7H$_2$O, 99.5%), PVA ([CH$_2$CH (OH)]$_n$, n = 1799) were purchased from Aladdin. Vanadium oxytriisopropoxide (C$_9$H$_{21}$O$_4$V, 97%) was purchased from Tstachi (Shanghai) into Industrial Development Co., Ltd, (Shanghai, China). Hydrochloric acid (HCl, 36-38%), isopropanol alcohol (C$_3$H$_8$O, 99.7%), sodium sulfate (Na$_2$SO$_4$, 99%), and boric acid (H$_3$BO$_3$, 99.8%) were obtained from Sinopharm Chemical Reagent, China. Each of these chemicals was used directly without any further purification. CNTFs were fabricated with a floating catalyst chemical vapor deposition method followed by shrinking with ethanol.

Preparation of carbon nanotube fibers (CNTFs)

The CNTFs were fabricated by two processes including of floating catalyst chemical vapor deposition (FCCVD) method and twisting method. The pristine CNT strip used for fabrication of CNTFs was synthesized at 1300 °C using ethanol and ferrocene as carbon source and catalyst via FCCVD process. The typical thickness, mechanical strength, and electrical conductivity of the pristine CNT strip are around 10 μm, 30-50 MPa, and 10^5 S/m, respectively. The CNTFs were fabricated by twisting a CNT strip via a fast and scale process and were used for current collector.

Materials characterization

The morphologies of the as-prepared samples were characterized by scanning electron microscopy (SEM; Hitachi S-4800, 5 kV). The microstructures of the samples were observed by transmission electron microscopy (TEM; FEI Tecnai G2 F20 S-Twin), and

high-resolution TEM images were acquired on an FEI Tecnai G2 20 high-resolution transmission electron microscope operating at an acceleration voltage of 200 kV. The chemical compositions of the samples were analyzed on an ESCALAB MKII X-ray photoelectron spectrometer (XPS) using non-monochromatized Mg Kα X-rays as the excitation source. X-ray diffraction (XRD) patterns were acquired on a Rigaku D/MAX2500 V system using Cu Kα radiation (λ = 1.5418 Å).

Measurements of electrochemical performance

The electrochemical performances of the ZIBs were evaluated by galvanostatic charge/discharge (GCD), cyclic voltammetry (CV), and electrochemical impedance spectroscopy (EIS) measurements on an electrochemical workstation (CHI 760E, Chenhua) in a two-electrode cell with an aqueous electrolyte containing 2 M $ZnSO_4 \cdot 7H_2O$. The EIS measurements were assumed between 10^{-2}-10^5 Hz with a voltage amplitude of 5 mV and open-circuit potential. The capacity (C), energy density (E), and power density (P) were calculated according to the following equations:

$$C_A = \frac{1}{3600}\frac{I\Delta t}{A} \tag{1}$$

$$E_A = C_A * V_p \tag{2}$$

$$P_A = 3600 * \frac{EA}{\Delta t} \tag{3}$$

$$C_V = \frac{1}{3600}\frac{I\Delta t}{V} \tag{4}$$

$$E_V = C_V * V_p \tag{5}$$

$$P_V = 3600 * \frac{EV}{\Delta t} \tag{6}$$

Where A and V are the total area and volume of the as-assembled ZIBs, respectively. I, Δt and V_p represent the discharge current, discharge time, and voltage platform,

respectively. The cycling performance tests were conducted with GCD measurements with a constant current density 8 mA cm^{-2} for 3500 cycles.
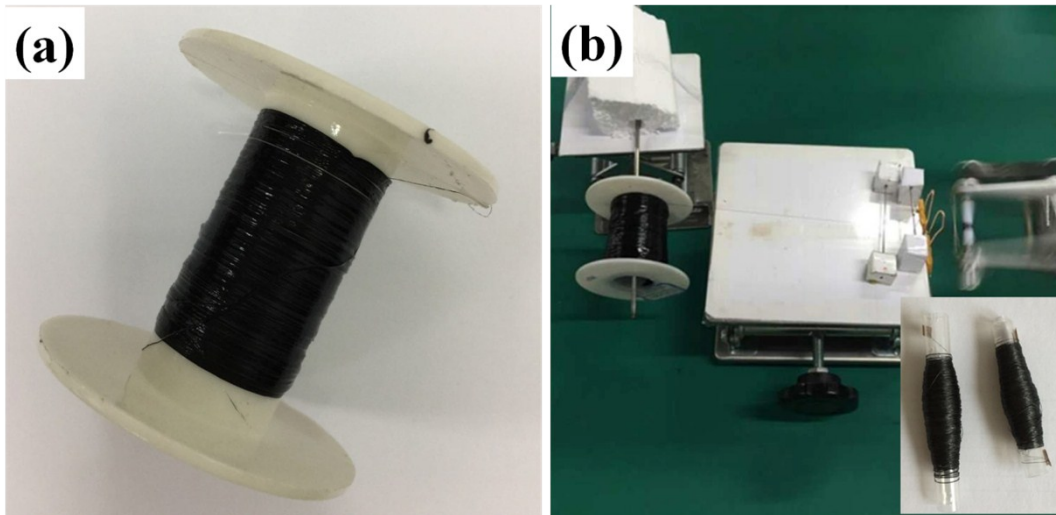
Figure S1 (a) Photograph of 60-m CNT strip. (b) Photograph of the experimental setup to prepare CNTF from a CNT strip. The insert shows the photograph of 60-m CNTF wrapped around a plastic tube.
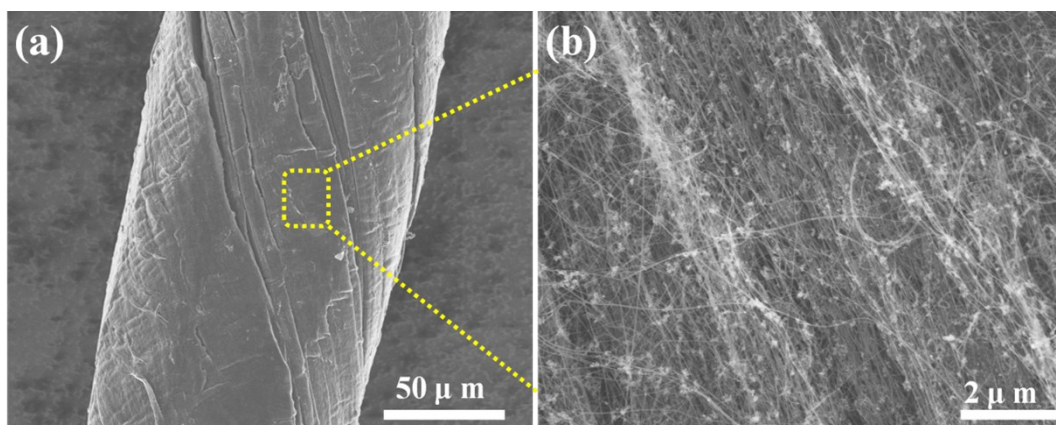
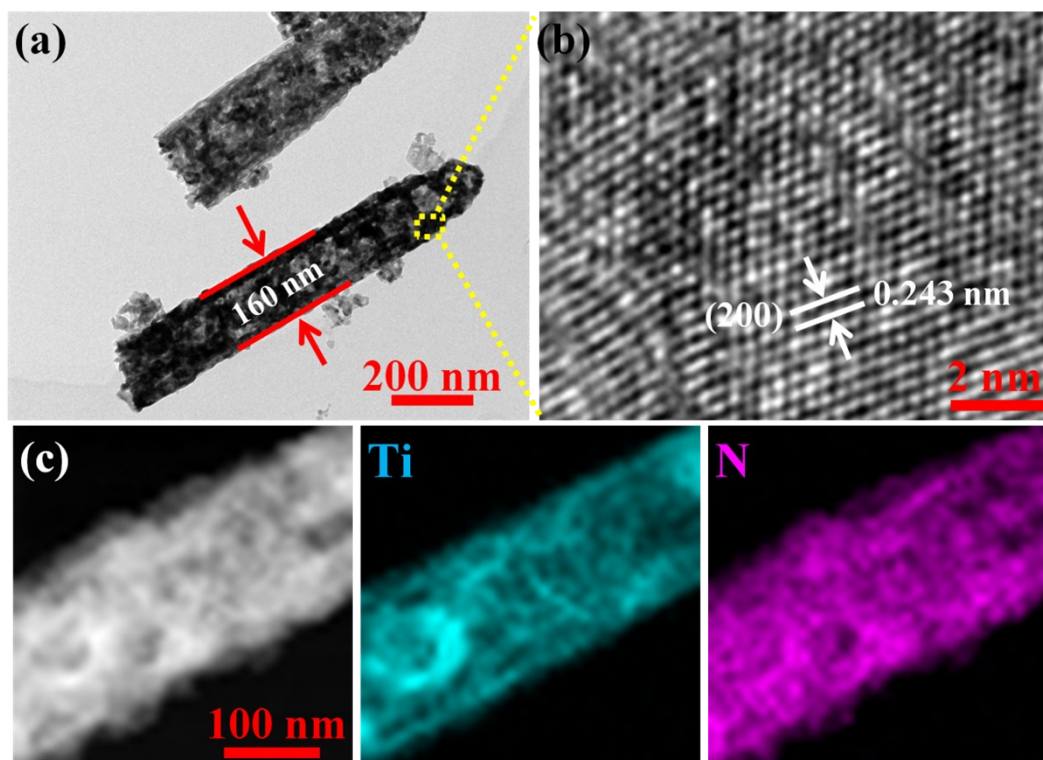**Figure S2** (a, b) SEM images of bare CNTF at different magnifications.

Figure S3 (a) Low-magnification TEM image of single TiN nanowire. (b) High-magnification of the red rectangle in panel a. (c) TEM image of single TiN nanowire and the corresponding EDS element mapping images.
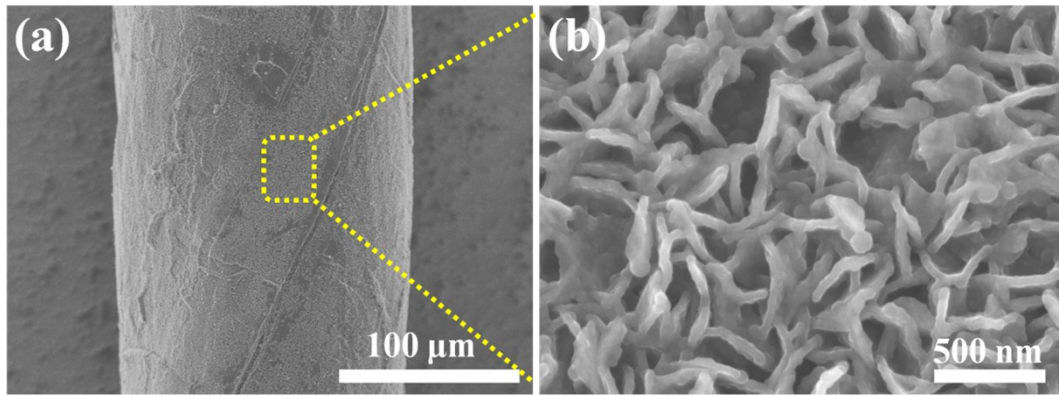
Figure S4 (a) SEM image of the V_2O_5 NSs grown on the CNTF surface at low magnification. (b) SEM image of the V_2O_5 NSs/CNTF at high magnification.
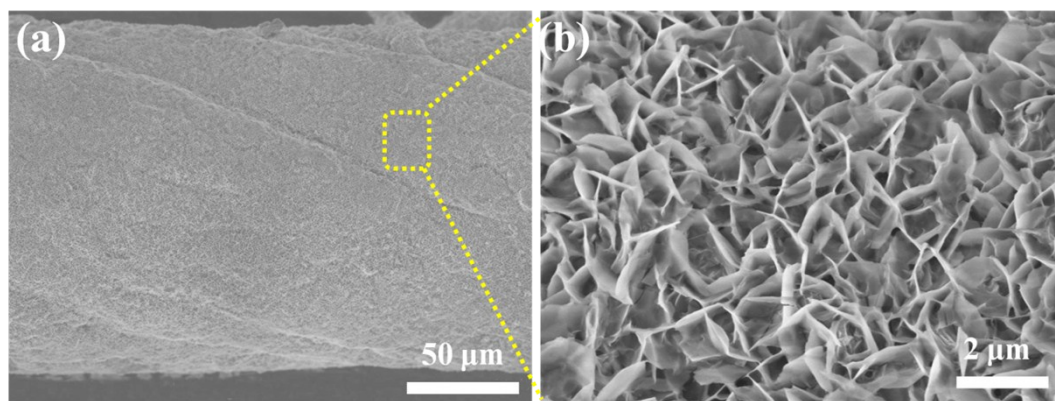
Figure S5 (a) SEM image of the Zn NSs/CNTF at low magnification. (b) SEM image of
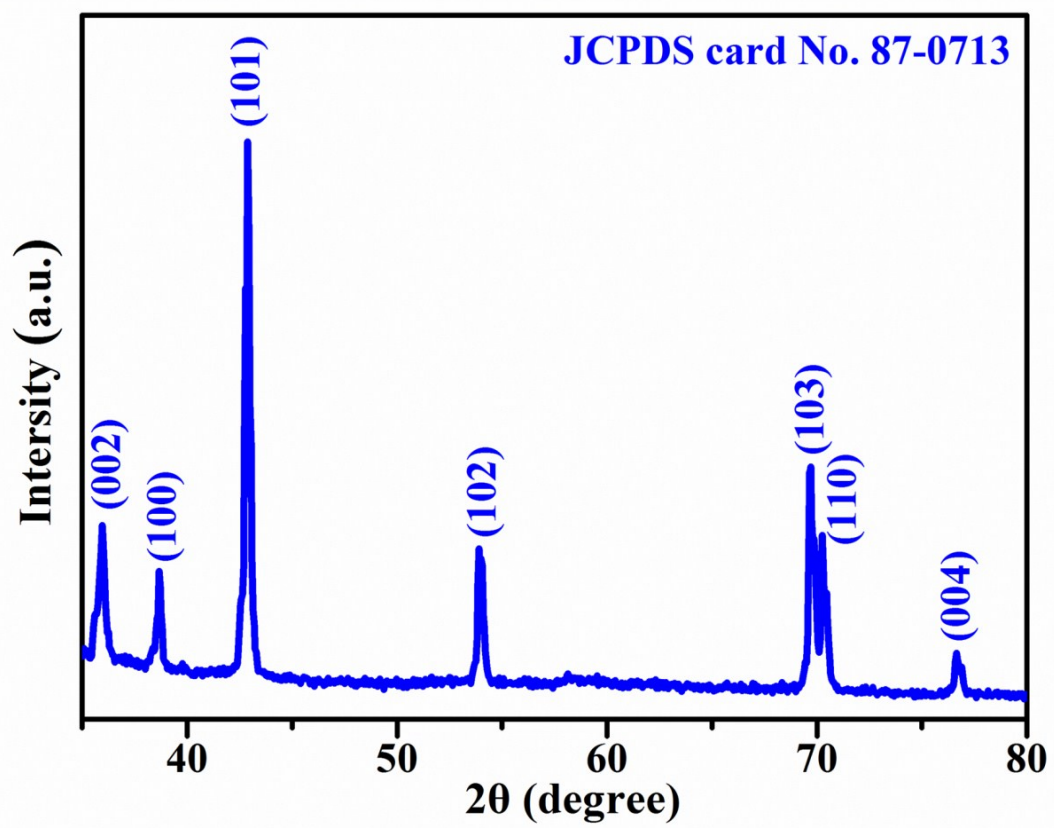
the Zn NSs/CNTF at high magnification.

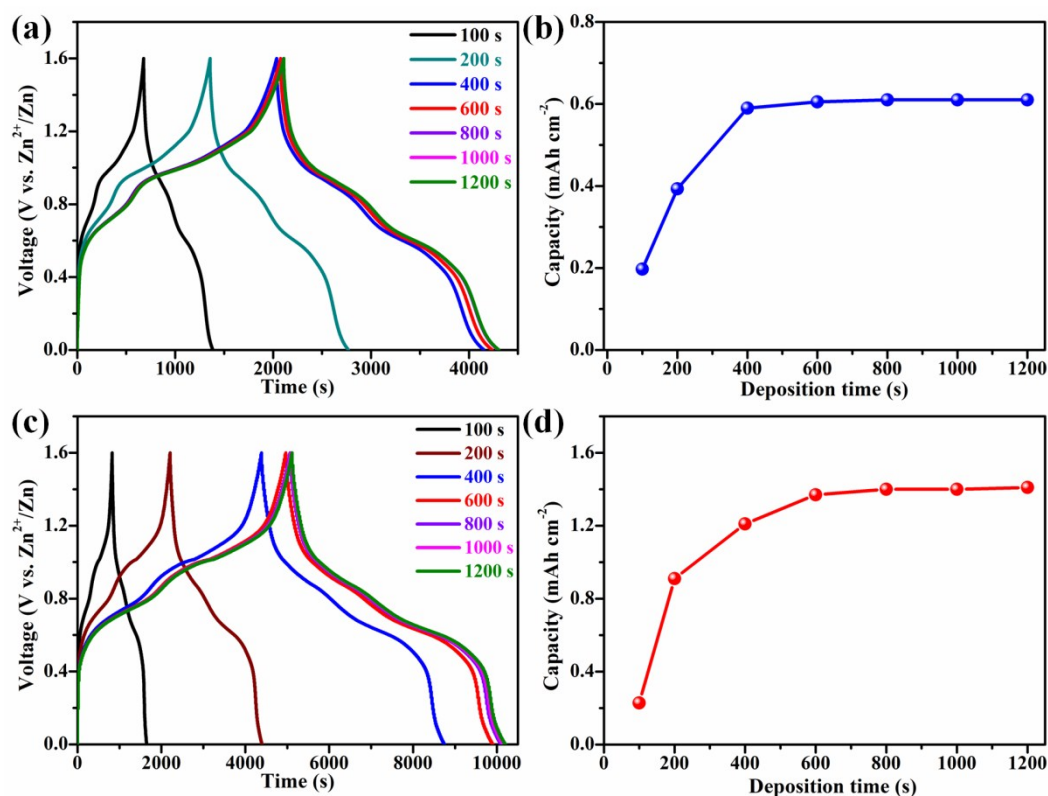**Figure S6** XRD partten of Zn NSs.

Figure S7 GCD curves of the (a) V_2O_5 NSs//Zn and (c) TiN@V_2O_5 NWAs//Zn batteries with different Zn deposition time at a current density of 1 mA cm^{-2}. The relastionship between the capacity of (b) V_2O_5 NSs//Zn and (d) TiN@V_2O_5 NWAs//Zn batteries and Zn deposition time.

As shown in Figure S7a and b, the capacity of the V_2O_5 NSs//Zn battery is increased when the Zn deposition time enhances from 100 s to 400 s. Subsequently, with the further increase the deposition time, the capacity of the V_2O_5 NSs//Zn battery remains almost unchanged, revealing that the deposition time of 400 s is sufficient for this battery. Furthermore, the variation tendency of the capacity for the TiN@V_2O_5 NWAs//Zn battery is similar to that of the V_2O_5 NSs//Zn battery. Moreover, the Zn deposition time of 600 s is sufficient for the TiN@V_2O_5 NWAs//Zn battery. Therefore, 600 s was chaoiced as the optimum Zn deposition time.
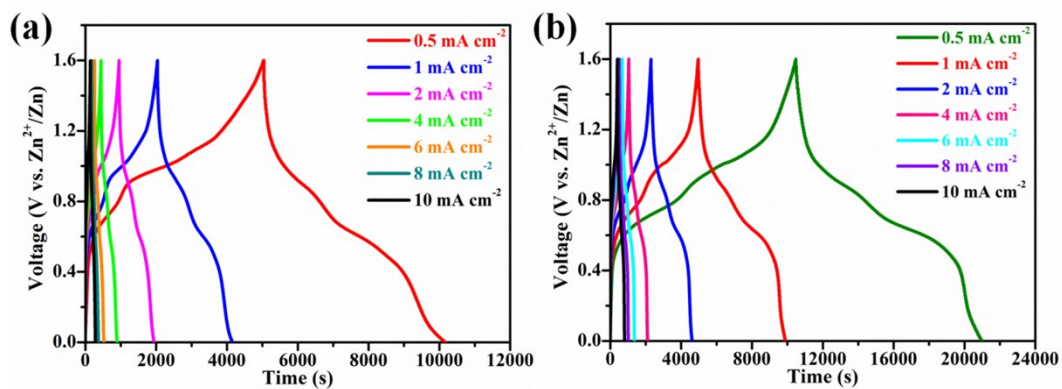
Figure S8 GCD curves of the (a) V_2O_5 NSs//Zn and (b) TiN@V_2O_5 NWAs//Zn batteries in the voltage (vs. Zn^{2+}/Zn) range from 0 to 1.6 V at current density from 0.5 to 10 mA cm^{-2}.
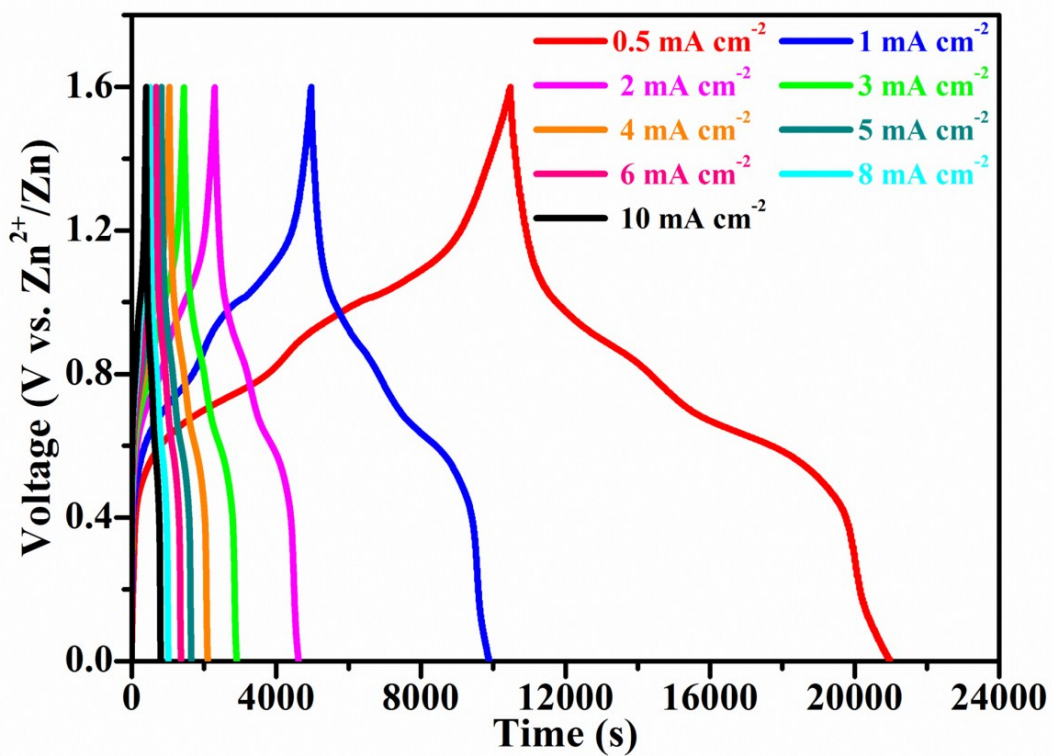
Figure S9 GCD profiles of the TiN@V_2O_5 NWAs//Zn battery in the voltage (vs. Zn^{2+}/Zn)

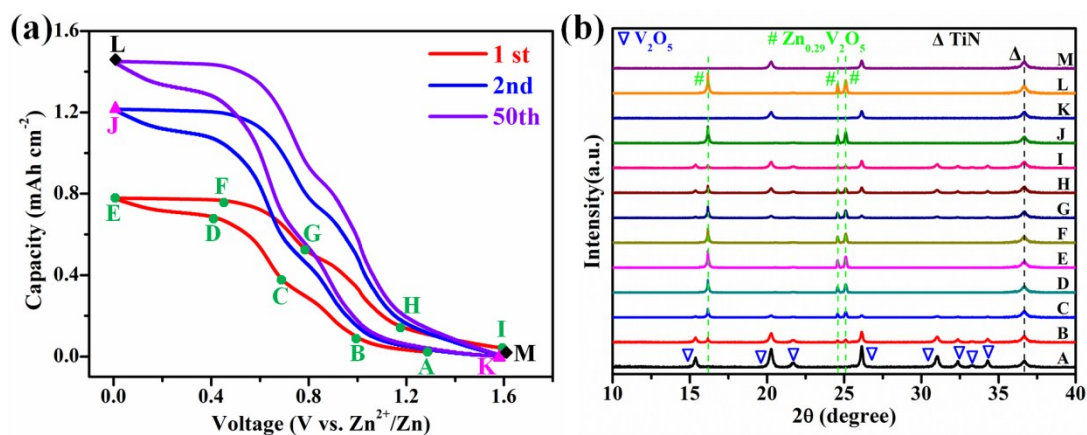range from 0 to 1.6 V at current density of 0.5, 1, 2, 3, 4, 5, 6, 8, and 10 mA cm^{-2}.

Figure S10 (a) Typical GCD curves of the aqueous TiN@V_2O_5 NWAs//Zn battery in the 1 st, 2nd, and 50th cycles at a current density of 0.5 mA cm^{-2}. The points A-M mark the states where data are collected for XRD analysis. (b) Ex-situ XRD patterns of the TiN@V_2O_5 NWAs cathode at selected states.

On the first discharging process (A → E), the diffraction peaks of V_2O_5 gradually weaken, and new phase peaks arise. The insertion of Zn^{2+} ions into V_2O_5 leads to the formation of a new layered phase of $Zn_{0.29}V_2O_5$ (JCPDS card No. 24-1480), confirming the intercalation of Zn^{2+} ions. After discharging to 0.7 V, the two mixed phases of V_2O_5 and $Zn_{0.29}V_2O_5$ exist simultaneously. On the discharging process from C to E, only one phase of $Zn_{0.29}V_2O_5$ is found, indicating full Zn^{2+} ions intercalation. Moreover, the subsequent charging process (E → I), the main diffraction peaks at 16.19°, 24.57°, and 24.92° gradually weaken, indicating the extraction of Zn^{2+} ions. After charging to 1.6 V, the $Zn_{0.29}V_2O_5$ phase is still observed while the pristine peaks of V_2O_5 can be partially recovered, indicating that partial Zn^{2+} ions are not fully extracted and the layered structure of V_2O_5 was reversible during the GCD process. In the 2nd and 50th cycles, the signals of layered compounds can reversibly strengthen/weaken upon Zn^{2+} ions insertion/extraction.
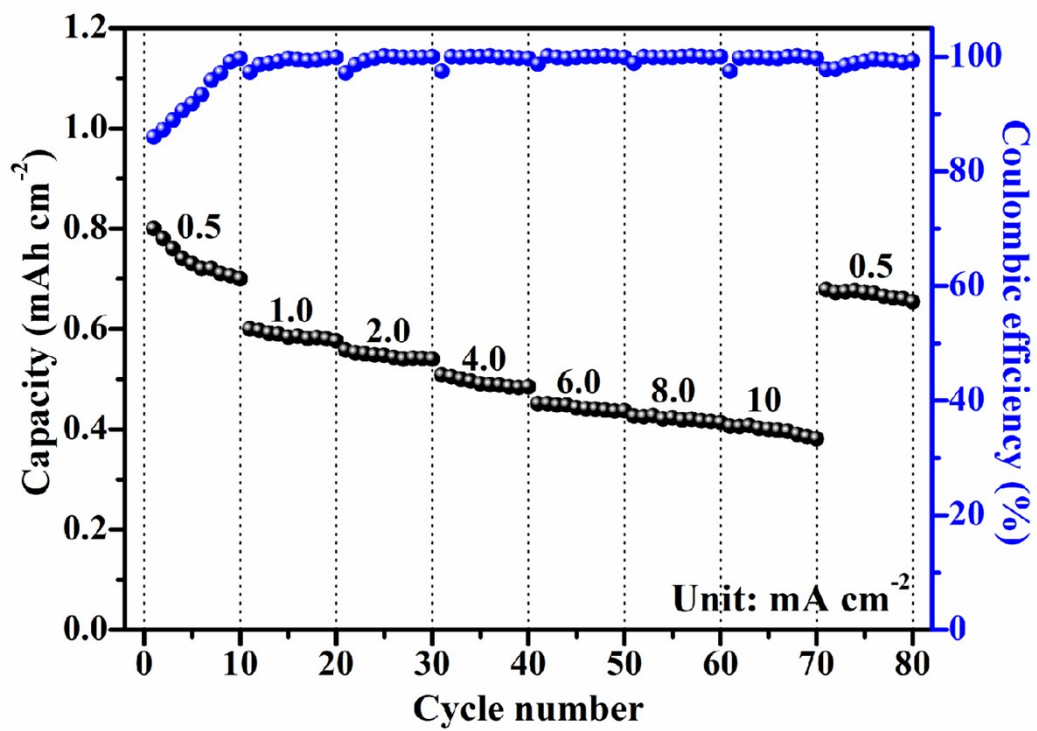
Figure S11 Rate capability and coulombic efficiency at various current densities of the
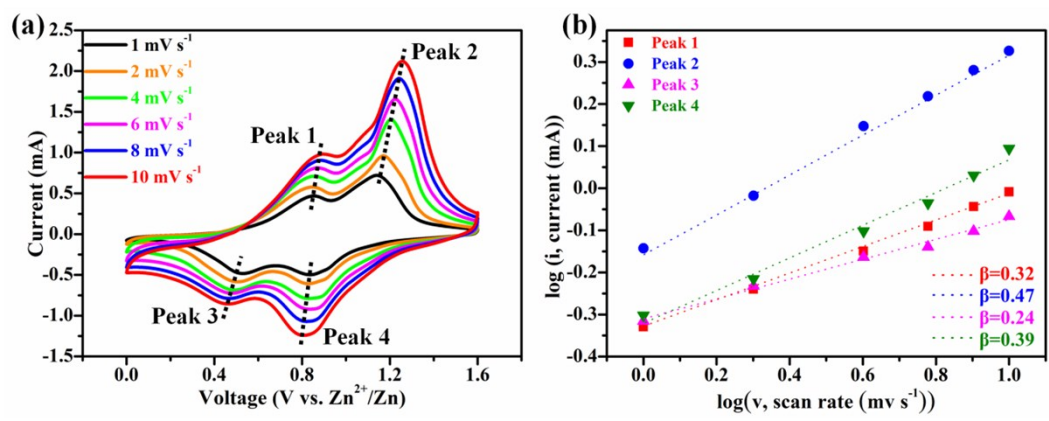
V_2O_5 NWAs//Zn battery.

Figure S12 (a) CV curves of the V_2O_5 NSs//Zn battery at various scan rates and (b) the corresponding plots of log (peak current, *i*) vs. log (scan rate, *v*) based on the CV files at different oxidation/reduction states.
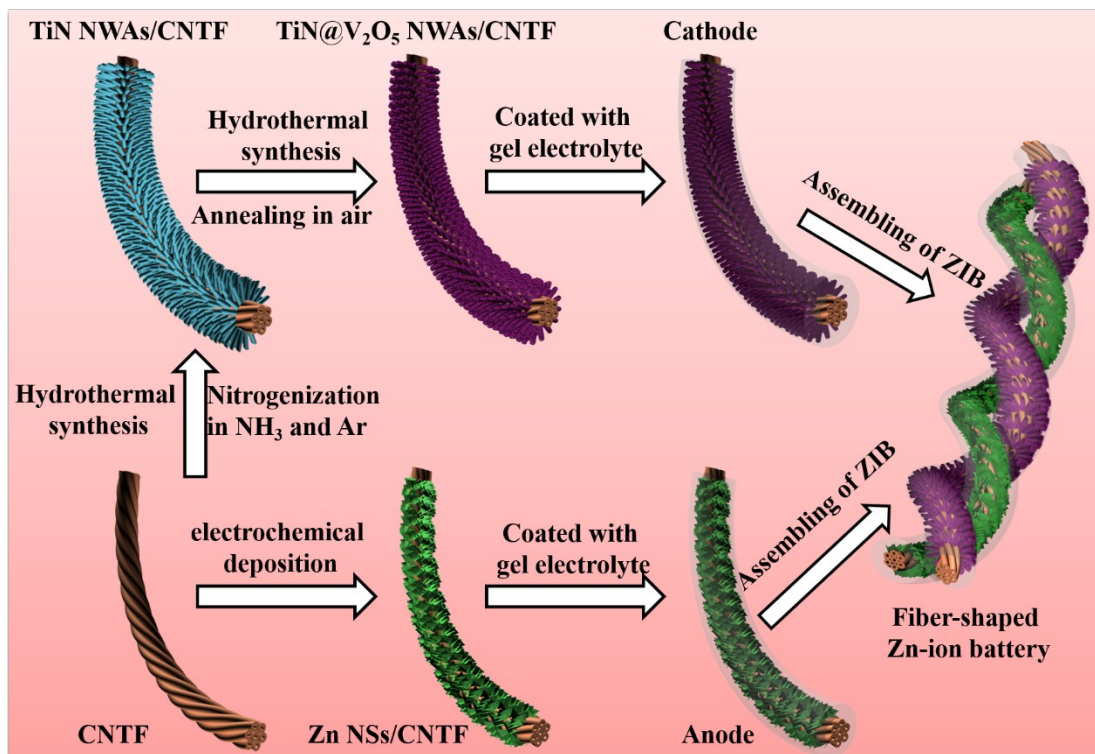
Figure S13 Schematics of the fabrication processes of the cathode and anode materials and the fiber-shaped Zn-ions battery.
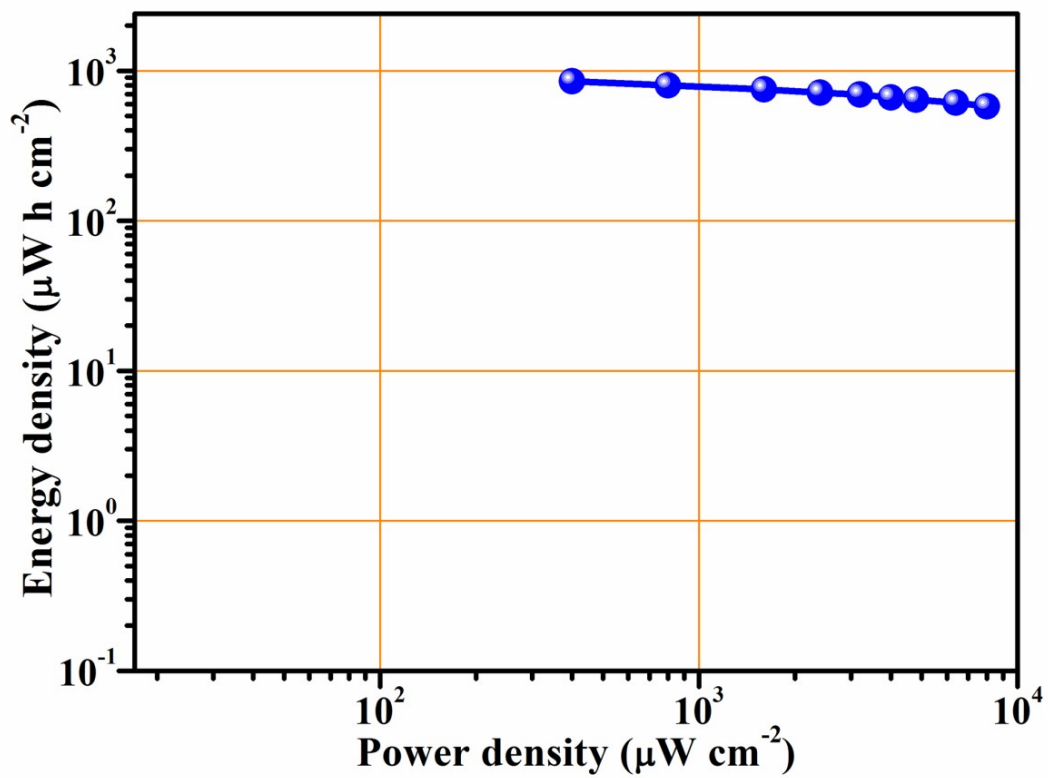
Figure S14 Areal energy and power densities of our as-assembled fiber-shaped all-solid-state TiN@V_2O_5 NWAs//Zn battery.
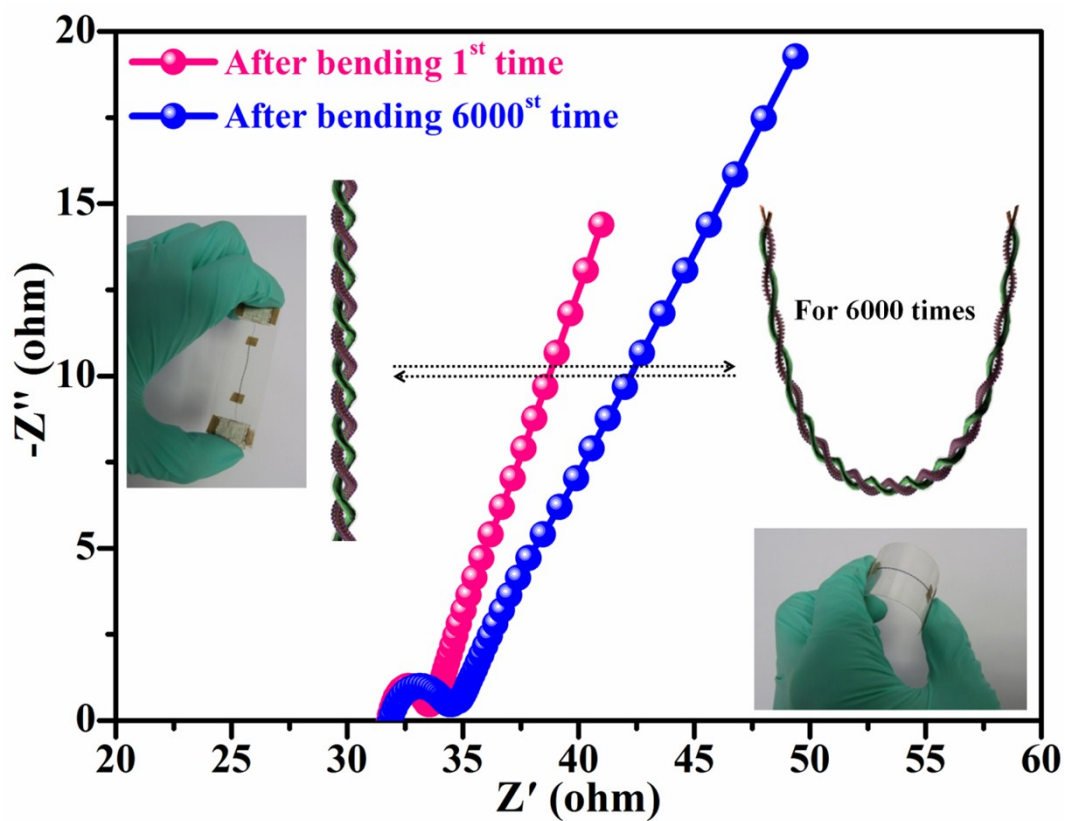
Figure S15 Nyquist plot of the as-assembled fiber-shaped ZIB at frequencies ranging from 10^{-2} to 10^5 Hz with a voltage amplitude of 5 mV at open-circuit potential after bending 1st and 6000th times (Insert shows the schematic diagrams and pictures of the fiber-shaped ZIB at a bending angle of 180° for 6000 cycles).

After the 1st and 6000th bending cycles, the equivalent series resistance values of our device are about 32.6 Ω and 33.6 Ω, indicating the enhancement of the ionic resistance of the electrolyte and the resistance of the active materials after the bending cycles. Furthermroe, the semicircle diameter related to charge transfer resistance also enlarges after 6000 bending cycles.
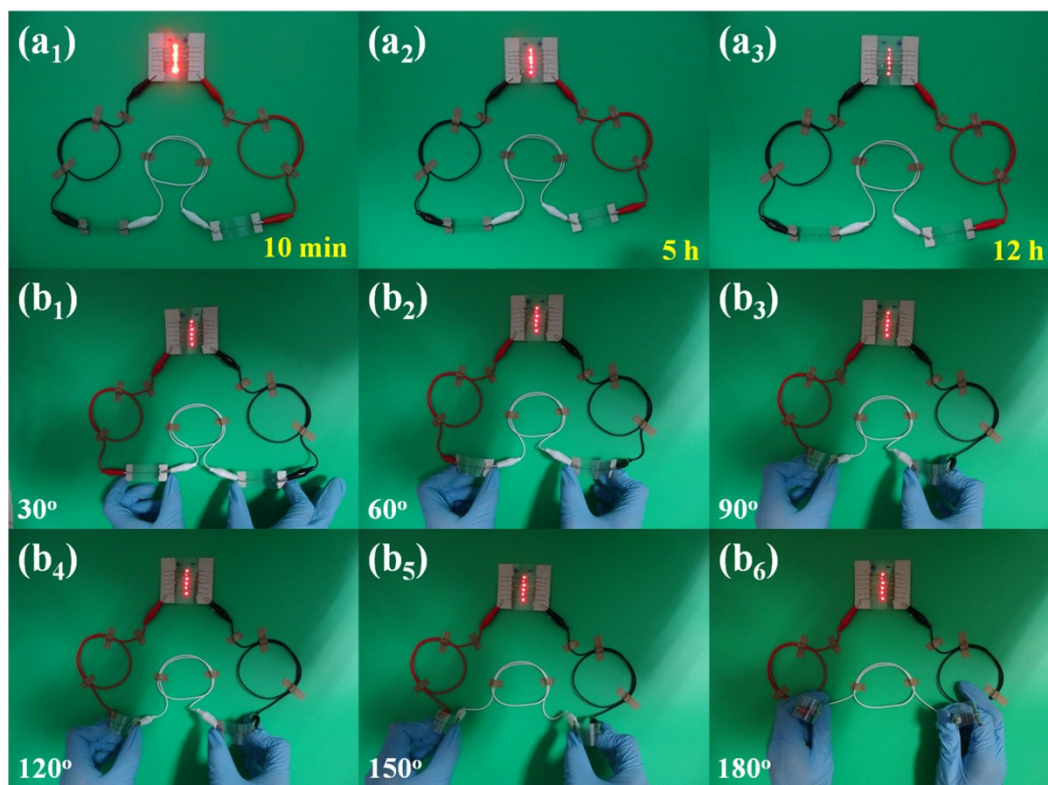
Figure S16 (a) Optical images of lightness of six red LEDs (powered by two fully charged as-assembled fiber-shaped ZIBs connected in series) changes with time: (a_1) 10 min, (a_2) 5h, and (a_3) 12h. (b) Optical images of the brightness of six red LEDs powered by two fully charged fiber-shaped ZIBs under different bending angle: (b_1) 30°, (b_2) 60°, (b_3) 90°, (b_4) 120°, (b_5) 150°, and (b_6) 180°.